Wide Band THz Transmitarray Antenna Based on Graphene Slotted Lattice

Mahdieh Ghaderi[1] and Pejman Rezaei[1]*

1. Electrical and Computer Engineering Faculty, Semnan University, Semnan, Iran.

Corresponding author: prezaei@semnan.ac.ir

***Abstract*— A novel terahertz (THz) Transmitarray antenna using an identically shaped slotted graphene lattice with wide bandwidth, is presented in this paper. The transmissive surface consists of graphene frequency selective surfaces (FSSs), using at THz frequencies. The graphene FSS consists of a double layer 11×11 unit cells array on two dielectric layers. The total thickness of the structure is only $\frac{\lambda_0}{2\cdot 14}$ at center frequency of 14 THz. The continuous slotted graphene sheets are connected to electrical bias, to control the chemical potential level of the graphene layers. A wideband, high gain, and high-efficiency transmitarray antenna using the presented graphene unit cells array, has been designed. Simulation results are shown the transmitarray antenna peak gain is 29.2 dB at 14 THz. The wideband transmitarray with a 3-dB gain bandwidth of about 30% and a 41.87% aperture efficiency is investigated.**

Index Terms — Frequency selective surface; Graphene lattice; Slot unit-cell; Transmission phase; Terahertz; Transmitarray antenna.

I. INTRODUCTION

Electromagnetic spectrum between microwave and optics, specified as THz band. In this frequency spectrum, due to the effect of strong skin, penetration of electromagnetic waves into metallic conductors, increased. Hence, the conductivity of metallic conductors decreased and generally led to a large loss in wave radiation. Therefore, in THz frequencies, novel optic materials including crystal photonic structures, plasmonic structures, and graphene material can be replaced. [1-5].

Recently, significant attention has been given to investigating structures that utilize graphene from microwave to the infrared band [6-14]. In this material, a complex conductivity can be continuously adjusted in a wide frequency band by shifting the electronic Fermi level via chemical or electronic doping, temperature T, and incident wave frequency [15-17]. Due to its initial characteristics, graphene structures have found many applications, including graphene-based nanomechanics, nanoelectronics, wireless communications, optical nanoantennas, and surface plasmon waveguides [18-27]. Furthermore, many devices in THz applications as modulators, filters, switches, and resonators realized by graphene [28-33].

Little skin effect and controllable chemical potential with electrostatic gate voltage, are two exclusive characteristics of graphene structures that make developments in graphene THz antennas.

Transmiarray Antennas (TAA) are high gain and wide bandwidth antennas, that can be used for THz applications using graphene structures [33-36]. Frequency Selective Surface (FSS) configurations can be used to make a graphene-based TAA with high gain radiation, for THz applications [37-39]. Graphene's conductivity depends on chemical potential and can be modified with an external bias voltage, since a material of interest for designing tunable THz antennas [40, 41]. The grids lattices, which are composed of periodic arrays of patches or apertures on a dielectric substrate, are used as basic elements for transmitarray design.

In this paper, a high-gain graphene TAA, consisting of an 11×11 array of identical slotted graphene unit cells, has been presented at 14 THz. Each unit cell consists of two graphene layers with identical shape slots separated by two substrate layers. Complete 360° transmission phase attained by varying the graphene slot length, while the transmission magnitude is near 1 (0 dB).

Graphene-based TAAs have been designed in different THz band center frequencies. In [42], a graphene sheet perforated between two dielectric layers constructed the 13×13 unit cells array of TAA. The suggested antenna introduces a maximum gain of 24.4 dB at 6 THz and 1.07 THz 1-dB gain bandwidth.

In [43], a graphene-based FSS reflectarray/transmitarray antenna was investigated at 1THz center frequency. The proposed structure consists of 11×11 elements with an extreme gain of 20.7 dB. Moreover, a graphene metamaterial TAA investigated from 0.74 to 0.94 THz in [44]. The transmission aperture is composed of 169 elements of three graphene metamaterial layers with a high gain of 18.5 dB.

In this research a high gain TAA is planned at 14 THz. The proposed antenna aperture surface consists of two graphene sheets slotted with identical patterns in the middle of the unit cells. The array of the graphene unit cells is on two SiO_2 substrate layers. Modifying the dimension of graphene slots can lead to a 360° phase distribution with high transmission

magnitude. A THz rectangular horn is used to feed the transmission aperture. The designed TAA radiation pattern simulated and exceeded high gain and desired aperture efficiency at the center frequency.

II. GRAPHENE OPTICAL SPECIFICATIONS

Surface plasmons (SPs) are electromagnetic (EM) waves that interact with charge excitations on the boundary between conductor and dielectric materials. These SP waves arise via the EM fields coupling to the conductor's electron plasma oscillated [1]. The plasma polaritons in graphene released new characteristics in plasmonics [45]. Even noble metals, which are commonly considered the most superior plasmonic materials, present challenges in terms of adjustment. Also, they exhibit significant ohmic losses, which limit their application to optical processing equipment. The diffusion of plasmons within doped graphene layers results in reduced losses and strong wave localization extending to the optical phonon frequency. In describing how graphene lattice acts over a specified frequency band, the state-of-the-art conductivity theory uses the following argument. The electrical conductivity of the graphene sheet depends on physical parameters, such as substrate thickness, chemical potential, and temperature. The effect of these parameter variations over the frequency band has thoroughly been investigated in this paper. Changing the chemical potential of the graphene results in a frequency shift. Adjusting the absorption frequency is feasible using an appropriate variation in the chemical potential, which can be performed by varying the gate voltage. The relation between graphene gate voltage and chemical potential is obtained from equation 1.

$$V_g = \frac{e\mu_c^2 h}{\pi\hbar^2 V_f^2 \varepsilon_0 \varepsilon_r} \quad (1)$$

In Eq. 1, V_g is the applied voltage on graphene, e (1.6×10^{-19}) is the electron charge, μ_c is the chemical potential, h is the thickness of the substrate, ε_r is the substrate permittivity, $\hbar$ is the reduced Plank's constant, and V_f is Fermi velocity in graphene. Changing the carrier concentration in graphene, the Fermi energy varied from 0.85×10^6 to 3×10^6. In this formula, Fermi velocity is assumed 1.1×10^6.

The graphene surface conductivity model was obtained from the well-known Kubo formula [3, 5]. The graphene permittivity can be extracted from $\varepsilon = -\frac{\sigma_{im}}{\omega\Delta} + \varepsilon_0 + i\frac{\sigma_{real}}{\omega\Delta}$ where σ_{real} and σ_{im} are defined as surface conductivity, and ω is the angular frequency. The real and imaginary parts of graphene permittivity at temperature T (300 Kelvin) are defined as follows:

$$\varepsilon_{reaal} = \frac{H\sigma_0}{\pi\omega\Delta} log\frac{|\hbar\omega+2\mu_c|}{|\hbar\omega-2\mu_c|} - \frac{4\mu_c}{\hbar\omega^2\Delta}\frac{\sigma_0}{\pi}\left(1-\frac{2\mu_c^2}{9t^2}\right) + \varepsilon_0 \quad (2)$$

$$\varepsilon_{im} = \frac{H\sigma_0}{2\omega\Delta}\left[tanh\left(\frac{\hbar\omega+2\mu_c}{4k_BT}\right) + tanh\left(\frac{\hbar\omega-2\mu_c}{4k_BT}\right)\right] \quad (3)$$

Where Δ=$1nm$ is the graphene thickness, k_B is the Boltzmann's constant, and t is electron relaxation time (t=0.1 ps). In Equation 2, σ_0 and H are defined as:

$$\sigma_0 = \frac{e^2}{4\hbar} \quad (4)$$

$$H = \left[1 + \frac{(\hbar\omega)^2}{(36t^2)}\right] \quad (5)$$

The temperature has a minimal effect on the imaginary part of conductivity and the frequency shift.

Fig. 1 shows the real and imaginary portions of the permittivity of graphene in three values of typical chemical potential.

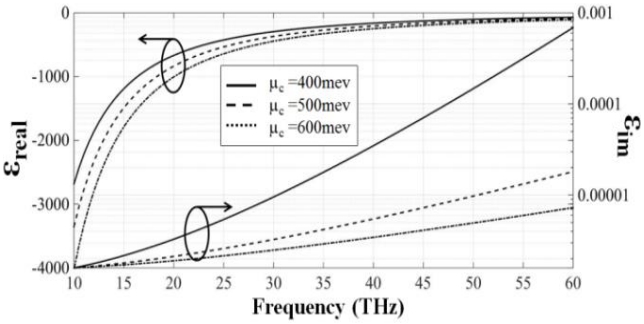

Fig. 1. Permittivity of graphene for three values of chemical potential.

III. GRAPHENE UNIT CELL PARAMETRIC DESIGN

The proposed TA aperture consists of double-layered unit cells, including two slotted graphene sheets on the top of two SiO_2 substrate layers, as displayed in Figure 2.

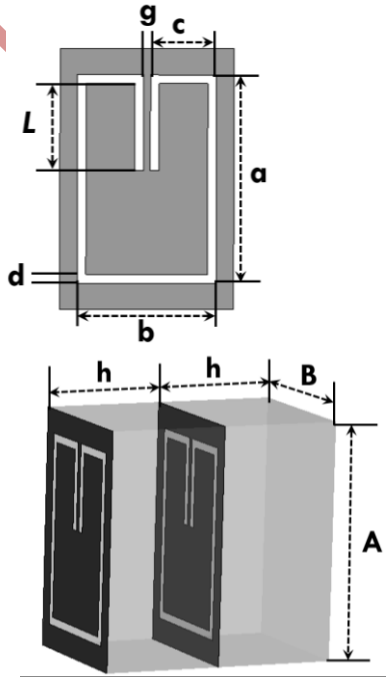

(a) (b)

Fig. 2. Schematic structure of the proposed unit-cell. (a) The patterned slot on the graphene sheet. (b) unit cell of dual layers slotted graphene sheet on two substrate layers.

The structure is optimized on dielectric layers with $\varepsilon_r = 3$ (SiO_2). A split ring resonator (SRR) slot is patterned on graphene layers. The unit cell dimensions as displayed in Fig. 2, are $A = 30\mu m$ and $B = 30\mu m$ and the thickness of $h =$

$5\mu m$. The dimensions of SRR are, $a = 24\mu m$, $b = 16\mu m$, $c = 7.6\mu m$, $d = 1\mu m$, and $g = 0.8\mu m$.

Hence, the total thickness of the structure achieved only $\frac{\lambda_0}{2\cdot 14}$ at center frequency of 14 THz.

To achieve a full transmission phase distribution, the length of $\boldsymbol{L}$ is adjusted within each unit cell as demonstrated in Figure 2.

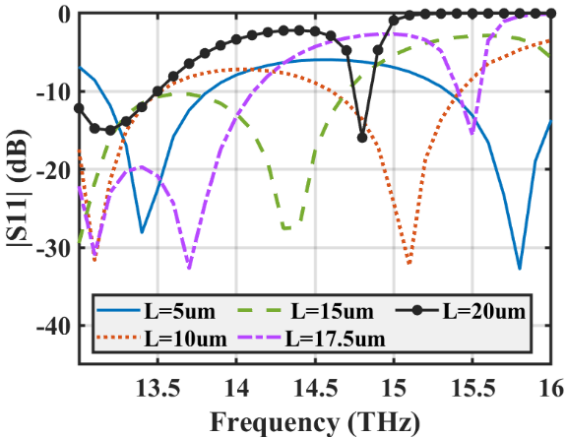

Fig. 3. The S-parameter of the proposed unit cell with chemical potential values, $\mu_c = 500\ mev$.

Figure 3 illustrates the reflection coefficient for the proposed structure at varying frequencies. The simulation results were performed using periodic boundary conditions with Floquet ports in CST Microwave Studio.

Figure 4 displays the parametric analysis of the proposed unit cell by changing length $\boldsymbol{L}$ at 14 THz. Implementing a full 360° phase shift arrangement with different $\boldsymbol{L}$ values results in uniform phase distribution along the antenna transmission aperture.

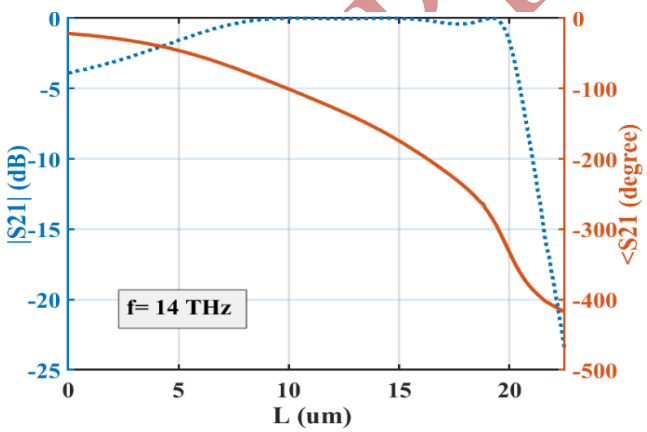

Fig. 4. Variation of the transmission coefficients of the proposed unit cells at 14 THz.

In Fig. 5, the S21 phases and magnitudes of the proposed unit cell are shown at three different frequencies in both upper and lower ranges. Changing $\boldsymbol{L}$ results in a 360-degree phase scan that can achieve almost complete transmission (0dB for |S21|), accordingly.

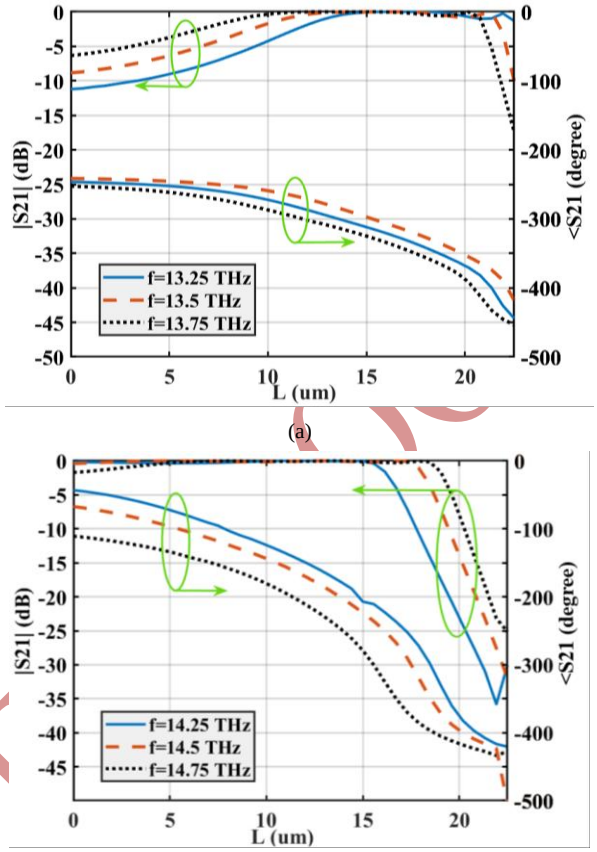

Fig. 5. The variation of transmission coefficients of suggested unit cells at (a) three lower frequencies, and (b) three upper frequencies.

In TA aperture design, the phase shift of each unit cell can be intended with the equation. 6 [46].

$$\psi(i,j) = \frac{2\pi f_0}{c}\left(R_{i,j} - \widehat{r_{i,j}}.\widehat{r_o}\right) + \psi_0 \qquad (6)$$

Where f_0 is the center frequency, c is 3×10^8, $\widehat{r_{i,j}}$ and $R_{i,j}$ is the position vector and distance of (i,j) element and the feed, respectively. In addition, $\widehat{r_o}$ is the unit vector oblique to the aperture. Fig. 6 shows the phase distribution of the proposed graphene TA aperture for 11×11 elements at 14 THz.

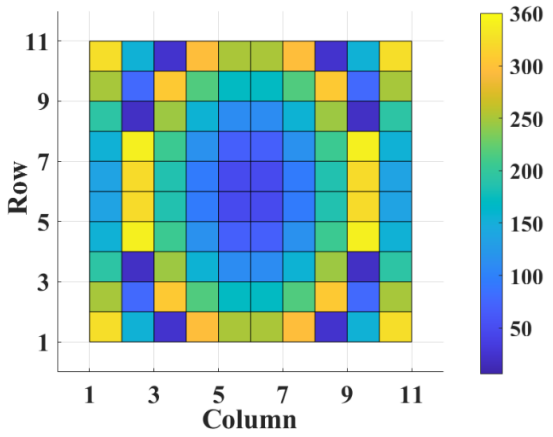

Fig. 6. Phase distribution on the proposed TA.

The TA arrangement is shaped by analyzing the relationship between transmission phase distribution and parametric properties of the unit cell.

IV. DESIGN OF THE GRAPHENE TAA

The proposed transmitarray aperture comprises an 11×11 unit cells array with a rectangular plane. The presented graphene transmitarray consists of two slotted graphene sheets implemented on two SiO_2 substrate layers. The graphene sheets are connected to gate voltage, to adjust the desired graphene chemical potential $\mu_c = 500\,mev$, as shown in Figure 7.

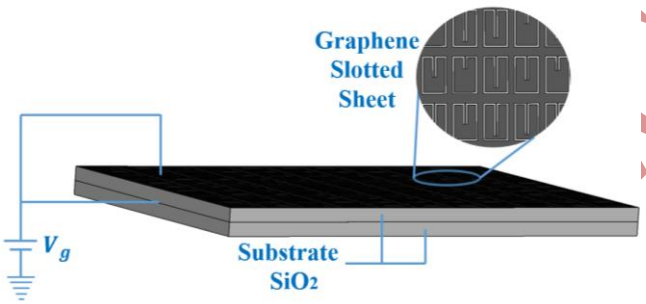

Fig. 7. The proposed 11×11 graphene transmitarray structure.

Substituting the parameters of the proposed structure in Eq. 1, the gate voltage needed for biasing presented graphene sheets, calculated $V_g = 21 \cdot 58\,v$. The proposed slotted graphene sheets are continuous since to fabricate the structure we need a proper graphene sheet and then cut the proposed slots on them.

Some fabrication methodologies for graphene have been discussed in recent years [47]. Predictably, the desired graphene transmitarray structure fabrication will be realized. A pyramidal horn antenna is designed in the desired frequency band as a feeding source. The far-field pattern of the presented horn feed at 14 THz can be defined with $cos^q(\theta_e)$ [46], with q=7 and, $\theta_e = 27^o$ the HPBW of the designed feed. The distance between the feed a TA, $\boldsymbol{F}$ can be calculated from Equation 7, as follows.

$$F = \frac{0.5D}{\tan\theta_e} \tag{7}$$

Where $\boldsymbol{D}$ is the biggest dimension in the aperture array, in the proposed design, F/D=0.98 is assumed and $F = 323.8um$, equal $15.11\lambda_0$.

The simulation results of the proposed TAA are shown in Fig. 8. The rectangular horn antenna with a maximum gain of 16.4 dB at 14 THz designed to feed the TAA, is shown in Fig. 8 (a). Additionally, the 3-D view of the far-field pattern of the designed feed antenna and proposed TAA are displayed in Fig. 8 (b, c). Fig. 8 (d), shows the reflection coefficients of the feed horn and TAA. Moreover, the co-polarization and cross-polarization radiation patterns of feed and TAA are shown in Fig. 8 (e). The peak gain of the proposed THz antenna is 29.2 dB with the SLL of -17.5 dB achieved at 14 THz.

In Fig. 8 (f), a comparison between the far-field co-polar patterns of the suggested antenna at 13.5, 14 and 14.5 THz, is presented.

The variations of peak gain and aperture efficiencies versus frequency for the proposed 11×11 TAA, are displayed in Figure 8.

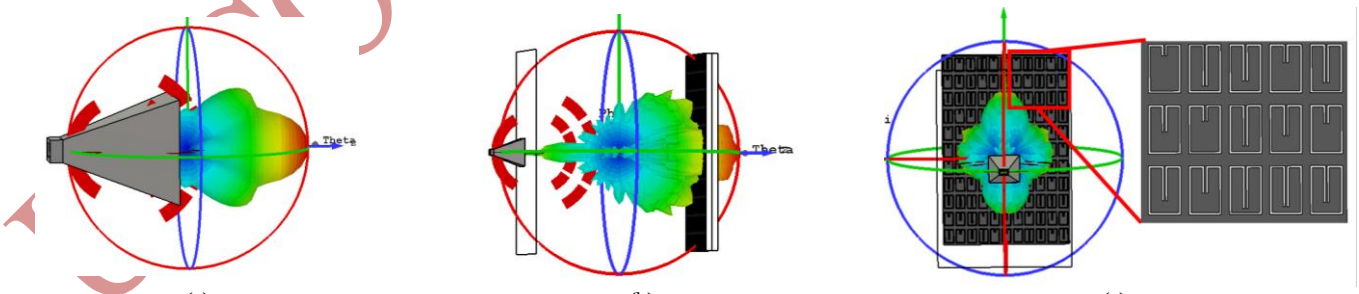

(a) (b) (c)

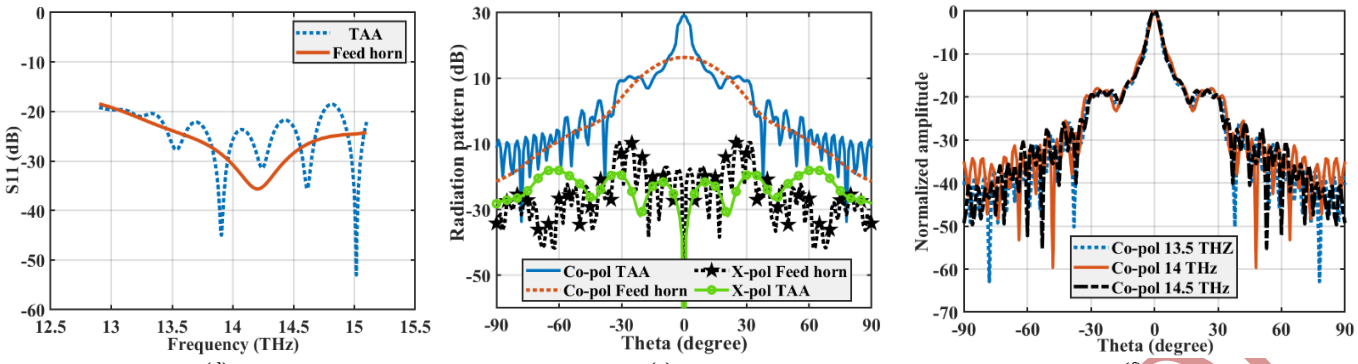

(d) (e) (f)

Fig. 8. (a) 3D view of the radiation pattern of the feed antenna, (b) 3D view of the far-field pattern of 11×11 proposed TAA, side view, (c) 3D view of the far-field pattern of 11×11proposed TAA, front view, (d) reflection coefficient of feed and proposed TAA, (e) Co-polarization and cross-polarization radiation pattern of feed and TAA, (f) normalized radiation pattern of proposed TAA at three frequencies.

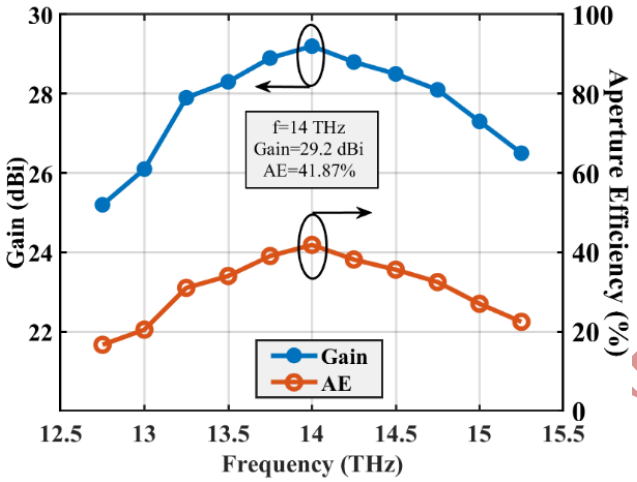

Fig. 9. Variation of gain and aperture efficiency of proposed TAA in different frequencies.

As shown in Figure 9, the 1-dB gain bandwidth is from about 13.5 THz to 14.75 THz, equal 8.9%, and 15.7% 3-dB gain bandwidth from 13.1 THz to 15.3 THz. The peak gain of 29.2 dB and maximum aperture efficiency, of 41.87% are achieved at center frequency, 14 THz. The design process of TAA, step by step, can be specified as a flowchart, shown in Figure 10.

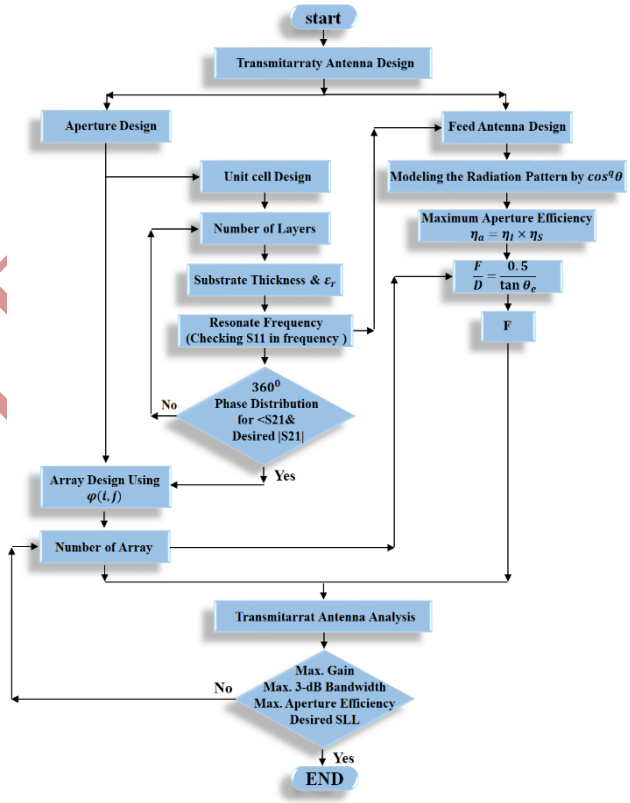

Fig. 10. Flowchart related to TAA design.

TABLE I
Comparison Between Planned Graphene TAA and the Reported Research.

Ref.	Frequency	Unit cell size (λ_0)	Layers	Substrate (ε_r)	Array	Aperture size (λ_0^2)	Max. Gain	Aperture Efficiency	3-dB Bandwidth
[42]	6THz	0.56	2 sub* layers + 1 gr** sheet	12	13×13	53	24.4dB	41.35%	16.66%
[43]	1THz	0.33	4 sub layers + 4 gr patch layers	3.45	11×11	13.177	20.7dB	49.23%	----------
[48]	6THz	0.5	1 sub layer + 2 gr patch layers	3.45	9×9	20.25	18.63dB	28.66%	6.8%

[49]	2.7THz	0.84	2 sub layers + 2 gr slotted layers + 1 gold layer	3.9	40×40	413.55	8.91dB	70.14%	----------
[50]	0.9THz	0.57	5 metallic layers + 4 air gaps	1	64×64	1330.8	35.96dB	25.96%	26.67%
[51]	0.31THz	0.434	2 metallic layers + 1 sub layer	3.323	14×14	36.9	19.15dB	17.5%	48.38%
[52]	0.87THz	0.435	2 metallic layers + 1 sub layer + 3 metallic vias	2.2	50×50	473	34.341	45.7%	----------
Proposed	14THz	Horizontal: 0.93 Vertical: 1.4	2 sub layers + 2 gr slotted layers	3	11×11	157.542	29.2dB	41.87%	15.7%

*sub: substrate **gr: graphene

Table I illustrates the comparison between the presented graphene TAA and some similar antenna revealed in recent years. The designed graphene THz antenna has the advantages of small size, wide frequency bandwidth, and high gain and efficiency at 14 THz. In recent years, research in the THz spectrum has been very interesting and developed rapidly. Hence, the proposed antenna will be able to be used in THz wireless communication systems, data traffic antennas, security imaging systems, biomedical imaging, and space telecommunications [53-55].

V. CONCLUSION

This paper introduces a high-gain graphene transmitarray antenna at THz frequencies. The proposed antenna's transmission aperture consists of the unit cells with two slotted graphene sheets on two SiO_2 substrate layers. The total thickness of the structure is only $\frac{\lambda_0}{2\cdot 14}$ at center frequency of 14 THz. The continuous slotted graphene sheets are connected to electrical bias to control the chemical potential of the graphene layers. The transmission aperture consists of an 11×11 unit-cells array with a rectangular dimension. A rectangular horn antenna is designed as feed in the proposed frequency band. The radiation pattern of the proposed TAA has a maximum power gain of 29.2 dB with a suitable SLL of about -17.5 dB at 14 THz. Hence, the 1-dB gain bandwidth and maximum aperture efficiency of the proposed structure are 8.9% and 41.87%, respectively.

Acknowledgment

The authors acknowledge the Semnan University. Also, the authors would like to thank the Editor and reviewers for their constructive comments.

Declaration of Competing Interest

The authors declare that they have no known competing financial interests or personal relationships that could have appeared to influence the work reported in this paper.

Funding

No funding was received for this research.

Data availability

All data generated or analyzed during this study are included in this published article.

REFERENCES

[1] S. A. Maier "Plasmonics: Fundamentals and Applications" 2007 Springer Science and Business Media LLC.
[2] A. Hamouleh-Alipour, S. Khani, M. Ashoorirad, R. Baghbani. Trapped multimodal resonance in magnetic field enhancement and sensitive THz plasmon sensor for toxic materials accusation. IEEE Sensors J. 2023; 13(2):14057-14066.
[3] S. Khani, M. Danaie, P. Rezaei, "Plasmonic all-optical modulator based on the coupling of a surface Plasmon stub-filter and a meandered MIM waveguide," Optical and Quantum Electronics, vol. 54, no. 12, pp. 849, 2022.
[4] A.H. Asl, M. Khajenoori, Green extraction in separation technology, CRC Press, 2021.
[5] S. Khani, M. Danaie, and P. Rezaei. "Plasmonic all-optical metal insulator-metal switches based on silver nano-rods, comprehensive theoretical analysis, and design guidelines." J. Computational Electron. 2021;20(1): 442-457.
[6] M. Jablan, H. Buljan, M. Soljačić, "Plasmonics in graphene at infrared frequencies" Physical Review B 80, 245435 (2009).
[7] F. H. L. Koppens, D. E. Chang, and F. Javier García de Abajo "Graphene plasmonics: A platform for strong light_matter interactions," Optoelectronics Research Centre, University of Southampton, Southampton SO17 1BJ, UK.
[8] S.M. Ebadi, S. Khani, Highly-miniaturized nano-plasmonic filters based on stepped impedance resonators with tunable cut-off wavelengths, Plasmonics 18 (4), 1607-1618, 2023.
[9] E. Einarsson, and J. Bird. "Active plasmonic antenna arrays for terahertz frequency communications," Defense Technical Information Center, (2023): 35.

[10] A.R. Jalalvand, Z. Rashidi, et al. “Sensitive and selective simultaneous biosensing of nandrolone and testosterone as two anabolic steroids by a novel biosensor assisted by second-order calibration,” Steroids, 189 (2023): 109138.
[11] P. Mahankali, S. Mondal, R. R. Thipparaju, and S. Mohandoss. "Graphene-based waveguide fed hybrid plasmonic terahertz patch antenna." Frequenz 78, no. 1-2 (2024): 71-78.
[12] Y. S. Cao, L. J. Jiang, and A. E. Ruehli. "An equivalent circuit model for graphene-based terahertz antenna using the PEEC method" IEEE Transactions on Antennas and Propagation, vol. 64, no. 4, April 2016.
[13] B. Khodadadi, M. Babaeinik, et al. "Triple-band metamaterial perfect absorber for refractive index sensing in THz frequency." Optical & Quantum Electronics 55(5) (2023): 431.
[14] P. Zamzam, P. Rezaei, Y. I. Abdulkarim, and O. M. Daraei. "Graphene-based polarization-insensitive metamaterials with perfect absorption for terahertz biosensing applications: Analytical approach." Optics & Laser Technology 163 (2023): 109444.
[15] T. Stauber, N. M. R. Peres, and A. K. Geim, “Optical conductivity of graphene in the visible region of the spectrum,” Phys. Rev. B 78, 085432 (2008).
[16] S. Hadipour, P. Rezaei, “A graphene-based triple band THz metamaterial absorber for cancer early detection,” Optical and Quantum Electronics, vol. 55, no. 13, pp. 1122, 2023.
[17] G. W. Hanson. "Dyadic Green’s functions and guided surface waves for a surface conductivity model of graphene." Journal of Applied Physics 103, no. 6 (2008).
[18] P. Zamzam, P. Rezaei, “Renovation of dual-band to quad-band polarization-insensitive and wide incident angle perfect absorber based on the extra graphene layer,” Micro and Nanostructures, vol. 168, pp. 207261, August 2022.
[19] S. Kiani, P. Rezaei, M. Fakhr, “On-chip coronavirus shape antenna for wideband applications in terahertz band,” Journal of Optics, vol. 52, no. 2, pp. 860-867, 2023.
[20] A. G. Olabi, M. A. Abdelkareem, T. Wilberforce, E.T. Sayed. "Application of graphene in energy storage device–A review." Renewable & Sustainable Energy Reviews 135 (2021): 110026.
[21] P. Zamzam, P. Rezaei, O. Mohsen Daraei, S. A. Khatami “Band reduplication of perfect metamaterial terahertz absorber with an added layer: Cross symmetry concept,” Optical and Quantum Electronics, vol. 55, 391, 2023.
[22] J. Soleiman Meiguni, and A. Ghobadi-Rad. "WLAN substrate integrated waveguide filter with novel negative coupling structure." Modeling and Simulation in Electrical and Electronics Engineering 1, no. 2 (2015): 15-18.
[23] N. Kiani, F. Tavakkol Hamedani, P. Rezaei, “Polarization controlling plan in graphene-based reconfigurable microstrip patch antenna,” Optik, vol. 244, 167595, pp. 1-10, 2021.
[24] Z. Ullah, G. Witjaksono, I. Nawi, N. Tansu, M. I. Khattak, and M. Junaid. "A review on the development of tunable graphene nanoantennas for terahertz optoelectronic and plasmonic applications." Sensors 20, no. 5 (2020): 1401.
[25] H. Yaghobi, M.R.M. Moghaddam. "Design processes linear permanent magnet electrical vernier machines for future research directions: A review." Modeling and Simulation in Electrical and Electronics Engineering 2 (2) (2022): 29-36.
[26] M. Karami, et al. “Modified planar sensor for measuring the dielectric constant of liquid materials.” Electronics Letters 53 (19) (2017): 1300-1302.
[27] R. Zheng, et al. "Ultra wideband tunable terahertz metamaterial absorber based on single-layer graphene strip." Diamond and Related Materials, 141 (2024): 110713
[28] S. Khani, M. Danaie, and P. Rezaei. "Fano Resonance using surface plasmon polaritons in a nano-disk resonator coupled to perpendicular waveguides for amplitude modulation applications." Plasmonics 16, no. 6 (2021): 1891-1908.
[29] S. M. Ebadi, S. Khani, and J. Örtegren. "Design of miniaturized wide band-pass plasmonic filters in MIM waveguides with tailored spectral filtering." Optical and Quantum Electronics 56, no. 5 (2024): 1-24.
[30] N. Korani, A. Abbasi, M. Danaie. “Band-pass and band-stop plasmonic filters based on Wilkinson power divider structure.” Plasmonics 19 (2) (2024): 733-742.
[31] S. Kiani, P. Rezaei. “Microwave substrate integrated waveguide resonator sensor for non-invasive monitoring of blood glucose concentration: Low cost and painless tool for diabetics.” Measurement 219 (2023): 113232.
[32] S. M. Ebadi, S. Khani, and J. Örtegren. "Ultra-compact multifunctional Surface plasmon device with tailored optical responses." Results in Physics 61 (2024): 107783.
[33] S. Khani, A. Farmani, and P. Rezaei. "Optical resistance switch for optical sensing." Optical Imaging and Sensing: Materials, Devices and Applications (2023): 83-122.
[34] S.H. Ramazannia, P. Rezaei, and F.T. Hamedani. "High-efficient wideband transmitarray antenna." IEEE Antennas and Wireless Propagation Letters 17, no. 5 (2018): 817-820.
[35] M. Ghaderi, and P. Rezaei. "Low profile wideband high gain transmitarray antenna for Ku band applications." Optics Communications (2024): 130701.
[36] H. Giddens, L. Yang, J. Tian, and Y. Hao. "Mid-infrared reflect-array antenna with beam switching enabled by continuous graphene layer." IEEE Photonics Technology Letters 30, no. 8 (2018): 748-751.
[37] S.H. Ramazannia Tuloti, P. Rezaei, F.T. Hamedani, “Unit-cell with flexible transmission phase slope for ultra-wideband transmitarray antennas,” IET Microwaves, Antennas & Propagation, vol. 13, no. 10, pp. 1522-1528, 2019.
[38] X. P. Chen, L. S. Wu, Y. Huang, K. X. Song, Y. P. Zhang, and J. F. Mao. "Terahertz transmit-array antenna with specific beamwidth based on thin film technology." IEEE Transactions on Antennas and Propagation (2024).
[39] Y. Yang, J. Deng, and Q. Cao. "Terahertz Transmitarray Antenna Using Rotated Z-shaped Elements." In IEEE 2020 Cross-Strait Radio Science & Wireless Technology Conference (CSRSWTC), pp. 1-3, 2020.
[40] L. A. Falkovsky, "Unusual field and temperature dependence of the Hall effect in graphene." Physical Review B 75, no. 3 (2007): 033409.
[41] V.P. Gusynin, S.G. Sharapov, J.P. Carbotte. "Magneto-optical conductivity in graphene." Journal of Physics: Condensed Matter 19, no. 2 (2006): 026222.
[42] M. Danaeifar, N. Granpayeh, N Asger Mortensen, and Sanshui Xiao " Equivalent conductivity method: straightforward analytical solution for metasurface-based structures " J. Phys. D: Appl. Phys. 48, IOP Publishing, 2015.
[43] W. M. Hassan, S. H. Zainud-Deen, and H. A. Malhat. "Compact multi-function single/dual-beam graphene lens antenna for terahertz applications." IEEE 33rd National Radio Science Conference (NRSC), pp. 41-48, 2016.
[44] W. T. Li, S. Sun, N. Qi, and X. Shi. “Reconfigurable graphene circular polarization Reflectarray/Transmitarray Antenna,” Frequenz 73, no. 3-4 (2019): 77-88.

[45] S. H. Zainud-Deen, A.M. Mabrouk, and H.A.E. Malhat. “Terahertz graphene based metamaterial transmitarray,” Wireless Personal Communications 100 (2018): 1235-1248.
[46] Huang, John, and Jose Antonio Encinar. Reflectarray antennas. John Wiley & Sons, 2007.
[47] R. Rudrapati. "Graphene: Fabrication methods, properties, and applications in modern industries." Graphene Production and Application 1 (2020).
[48] H. A. Malhat, S. H. Zainud-Deen, and S. M. Gaber. "Circularly polarized graphene-based transmitarray for terahertz applications." IEEE XXXIth URSI General Assembly and Scientific Symposium (URSI GASS), pp. 1-4, 2014.
[49] A. Shubham, D. Samantaray, S. K. Ghosh, Smrity Dwivedi, and Somak Bhattacharyya. "Performance improvement of a graphene patch antenna using metasurface for THz applications." Optik, 264 (2022): 169412.
[50] Z. W. Miao, Z. Liu, Z. C. Hao, Y. Zeng, D. Zhu, J. H. Zhao, C. Y. Ding, L. Cheng, L. Zhao, W. Hong. "A 1.0-THz High-Gain Metal-Only Transmit-Array Antenna Based on High-Precision UV-LIGA Microfabrication Technology." IEEE Transactions on Terahertz Science and Technology (2023).
[51] X. P. Chen, L. S. Wu, Y. Huang, K. X. Song, Y. P. Zhang, and J. F. Mao. "Terahertz Transmit-Array Antenna with Specific Beamwidth Based on Thin Film Technology." IEEE Transactions on Antennas and Propagation (2024).
[52] Z. W. Miao, Z. C. Hao, D. Q. Yu, C. Y. Ding, and F. Wu. "A W-band high-gain bilayer transmit-array antenna employing Huygens’ resonance." IEEE Antennas and Wireless Propagation Letters 22, no. 5 (2023): 1184-1188.
[53] A. Y. Pawar, D. D. Sonawane, K. B. Erande, and D. V. Derle. "Terahertz technology and its applications." Drug Invention Today 5, no. 2 (2013): 157-163.
[54] S. Shi, S. Yuan, J. Zhou, and P. Jiang. "Terahertz technology and its applications in head and neck diseases." IScience 26, no. 7 (2023).
[55] J. Ma, Y. Yang, B. Li, and H. Guerboukha. "Application of Terahertz Frequency in Substance Detection and Recognition." Frontiers in Physics 10 (2022): 959847.